

Learning phase transitions by siamese neural network

Jianmin Shen^{1,2}, Shiyang Chen^{2,3,*}, Feiyi Liu^{2,4,5,+}, Youju Liu¹, and Wei Li²

¹School of Engineering and Technology, Baoshan University, Baoshan 678000, China

²Key Laboratory of Quark and Lepton Physics (MOE) and Institute of Particle Physics, Central China Normal University, Wuhan 430079, China

³Department of Physics, Swansea University, SA2 8PP, Swansea, United Kingdom

⁴School of Physics and Electronic Science, Chuxiong Normal University, Chuxiong 675000, China

⁵Institute for Physics, Eötvös Loránd University, 1/A Pázmány P. Sétány, H-1117, Budapest, Hungary

*SY.Chern@Swansea.ac.uk

+fyliu@cxtc.edu.cn

ABSTRACT

The wide application of machine learning (ML) techniques in statistics physics has presented new avenues for research in this field. In this paper, we introduce a semi-supervised learning method based on Siamese Neural Networks (SNN), trying to explore the potential of neural network (NN) in the study of critical behaviors beyond the approaches of supervised and unsupervised learning. By focusing on the (1+1) dimensional bond directed percolation (DP) model of nonequilibrium phase transition, we use the SNN to predict the critical values and critical exponents of the system. Different from traditional ML methods, the input of SNN is a set of configuration data pairs and the output prediction is similarity, which prompts to find an anchor point of data for pair comparison during the test. In our study, during test we set different bond probability p as anchors, and discuss the impact of the configurations at this anchors on predictions. More, we use an iterative method to find the optimal training interval to make the algorithm more efficient, and the prediction results are comparable to other ML methods.

Introduction

With the rapid progress of the computer field in the past decade, machine learning (ML) has been explosively applied in various fields of science^{1,2}. By the great power of feature capture and classification, ML has brought new inspiration to the study of statistical physics and proven to be an effective tool for identifying and classifying different phases³⁻⁷. Through training process, ML algorithms can learn the underlying patterns and laws of phase transition from the input configurations of a given system, enabling them to make predictions in test data. Additionally, ML algorithms can automatically extract and select the most relevant features, which are valuable for reducing the complexity of high-dimensional phase transition data.

The mainly types of ML method applied to study phase transitions are supervised learning^{5,8-11}, unsupervised learning^{6,11-16}, and semi-supervised learning¹⁷⁻²¹. For supervised learning, the input data for training needs to be labeled, which commonly used to identify or classify the phases of matter. For unsupervised learning, the labeling of the order parameter is not required, such as the methods of principal component analysis (PCA)^{12,16,22}, t-distributed stochastic neighbor embedding (T-SNE)²³ or nonlinear autoencoder (AE)^{11,12,16,23}, for clustering and dimensionality reduction. Recently, semi-supervised learning, especially transfer learning (TL) also has been proved as a good choice to detect critical points and calculate critical exponents²⁰, even determining the type of phase transition²¹. With the input of mixing both labeled and unlabeled data, methods of TL can transform unlabeled data in target domain into labeled data in source domain by training, which only use a limited labeled set for the purposes of prediction. Although the methods of ML are dazzling, all of them are not fully perfect. For example, supervised learning must time-consumingly label the data; unsupervised learning is hard to fully identify the dynamic features with limited data; semi-supervised learning is very sensitive to the input, which always need to be preprocessed. Therefore, it is still imperative to find a more complete and efficient method of ML to study phase transitions.

Siamese neural network (SNN)^{24–26}, also called twin NN, is a specialized architecture usually consisting of two parallel identical neural networks (NN) that share their weight for the purposes of assessing or comparing the similarity between two input objects. SNN is not simply classified into supervised learning, unsupervised learning or semi-supervised learning, but a flexible structure that fill them in. It is widely used in computer vision for face recognition²⁷, target tracking²⁸ and image retrieval²⁹, and also shows its power in natural language processing (NLP) for text matching tasks³⁰. In the study of phase transition, Patel *etal*³¹ introduced a SNN technique of unsupervised learning to identify phase boundaries in Ising-type systems and Rydberg atomic arrays, showing its ability to learn about multiple phases without knowing about their existence. As the preliminary attempt, SNN is proved as a valuable tool for discovering new and unfamiliar phases of matter, and worth for further application and exploration.

Inspired by this, we apply a new SNN algorithm based on semi-supervised learning to study the critical behaviors of phase transition. In this method, we divide input configurations to two separate sets for training. By choosing an anchor for configurations, the SNN would determine whether this samples belong to the same set through training, which gives the power to judge phases and find critical point. For test, we focus on the model of (1+1)-dimensional bond directed percolation (DP)^{32–34}, belonging to the most important universality class of nonequilibrium phase transitions, the DP universality class^{35–37}. We not only predict the critical point of the DP model through the SNN, but also calculate the critical exponent by the data collapse method^{38,39}. Further, we discuss the impact of anchor point selection on results, and find the optimal interval of training set to achieve more accurate predictions. By doing so, we hope to enhance the effectiveness and reliability of the SNN as a new tool in the study of phase transitions.

The remaining content of this paper is structured in the following manner. In Section 1, we have introduced the directed percolation model. Section 2 gives the methods of SNN and the data set for study. Section 3 shows the estimate critical probabilities of SNN and also the prediction of spatial correlation exponent ν_{\perp} . In Section 4, we discuss the case of chosen anchor in critical region, and the impact of the training set on the results. Section 5 is a summary of this work.

1 Model

1.1 The directed percolation model

As the most prominent universality class of absorbing phase transition, DP describes percolation of one direction along that the system falls into inactive state where the time evolution stops. It is utilized to investigate various phenomena including the propagation of epidemics⁴⁰, forest fires⁴¹, and traffic flow⁴², etc. In past decades, a various of methods has been applied to study DP models, such as mean-field theory⁴³, renormalization groups⁴⁴, field theory approach⁴⁵ and numerical simulations⁴⁶ and so on. Some ML approaches have also been tried recently and shown their own strengths^{20,47}. Since the models of DP universality class include unitary or binary random reaction processes, which may contain diffusion or non-diffusion motions, only the critical exponents are common and the position of the phase transition may vary. In our work, we use a SNN based algorithm to study the (1 + 1)-dimensional bond DP, one of the simplest cases of DP universality class.

Fig. 1 illustrates the configurations of (1+1)-dimensional DP on the square lattice of size $L = 500$ with the evolution time step $t = 500$. Starting from a fully occupied lattice, a bond is formed at the time step with probability p from an existing bond, which can be interpreted as a reaction-diffusion mechanism of interacting particles with the active particle A and the empty site \emptyset :



By the arrows, this system evolves with the following rules:

$$s_i(t+1) = \begin{cases} 1 & \text{if } s_{i-1}(t) = 1 \text{ and } z_i^- < p, \\ 1 & \text{if } s_{i+1}(t) = 1 \text{ and } z_i^+ < p, \\ 0 & \text{otherwise,} \end{cases} \quad (2)$$

where $s_i(t)$ is the state of site i at time t and p is the bond probability of a connection between two adjacent sites. $z_i^{\pm} \in (0, 1)$ is a random number taken from an uniform distribution. From the definitions above, the configuration of the system can be determined by the states of all sites.

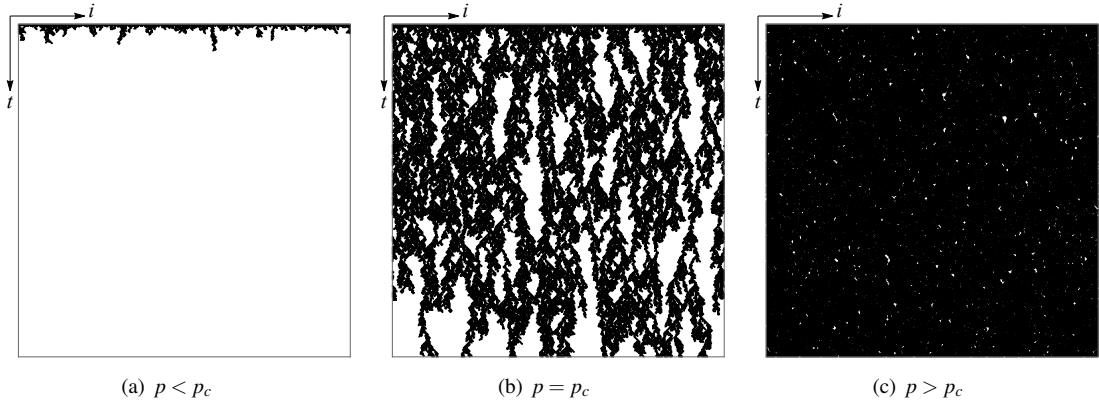


Figure 1. Configurations of the (1+1) dimensional bond DP corresponding to three different bond probabilities $p = 0.5, 0.6447$ and 0.8 respectively.

The models of DP universality class also has their own independent critical exponents. The order parameter of the (1+1)-dimensional bond DP close to the critical point p_c can be expressed by the steady-state particle density ρ_a according to the critical exponent β as³⁵,

$$\rho_a(p) \sim (p - p_c)^\beta. \quad (3)$$

In this steady state, the system also obeys the following power-law expressions of spatial and temporal correlation length:

$$\xi_\perp \sim |p - p_c|^{-\nu_\perp}, \quad \xi_\parallel \sim |p - p_c|^{-\nu_\parallel}, \quad (4)$$

where ν_\perp and ν_\parallel are the spatial and temporal correlation exponent.

In this paper, we use the the full configurations of the (1+1)-dimensional DP shown in Fig. 1 as input to the SNN algorithm. To generate the configurations, we use periodic boundary conditions, and originally starts with fully occupied lattice (explained in our previous study²⁰). The characteristic temporal length $t_c \sim L^{z/d}$ is set by the dynamical exponent $z = 1.580(1)$ and spatial dimension $d = 1$, to ensure the stable results³⁵.

2 Method

2.1 The Siamese Neural Network (SNN) method

The SNN is a type of deep learning model commonly used for tasks involving metric learning and similarity comparison²⁴. In various applications, SNNs are frequently employed to analyze pairs of input data, such as images, text, or voice²⁴. It works by creating multiple parallel sub-networks, known as "Branches", which share the same structure and weights. By feeding each input data through the NN of these branches for feature extraction, the SNN can calculate the similarity scores between them using metric functions like Euclidean distance or cosine similarity. The significant advantage of SNN is the capability to acquire adaptable feature representations while training, which enables the NN to achieve high performance even on datasets having some degree of variability. Additionally, SNN can be trained end-to-end by back-propagation algorithms, which allows the entire NN to autonomously learn feature representations and measures of similarity.

The specific framework of SNN used in our work to study phase transition of the (1+1)-dimensional DP is shown in the Figure 2. We use the raw configurations of $L = 8, 16, 32, 48$ and 64 as input, and the details of dataset selection will be given in Section 2.2. The input is a set of data pairs (S_i, S_j) , S_i enters one branch in the framework, and S_j enters the other. S_i and S_j are two different configuration samples of the same type of data. Taking the branch with S_i as an example, the input S_i is flattened into one-dimensional data and fed into an fully connected (FC) layer of 500 neurons with a *ReLU* activation function. Here we also set a Batch Normalization (BN) to avoid over-fitting and speed up the

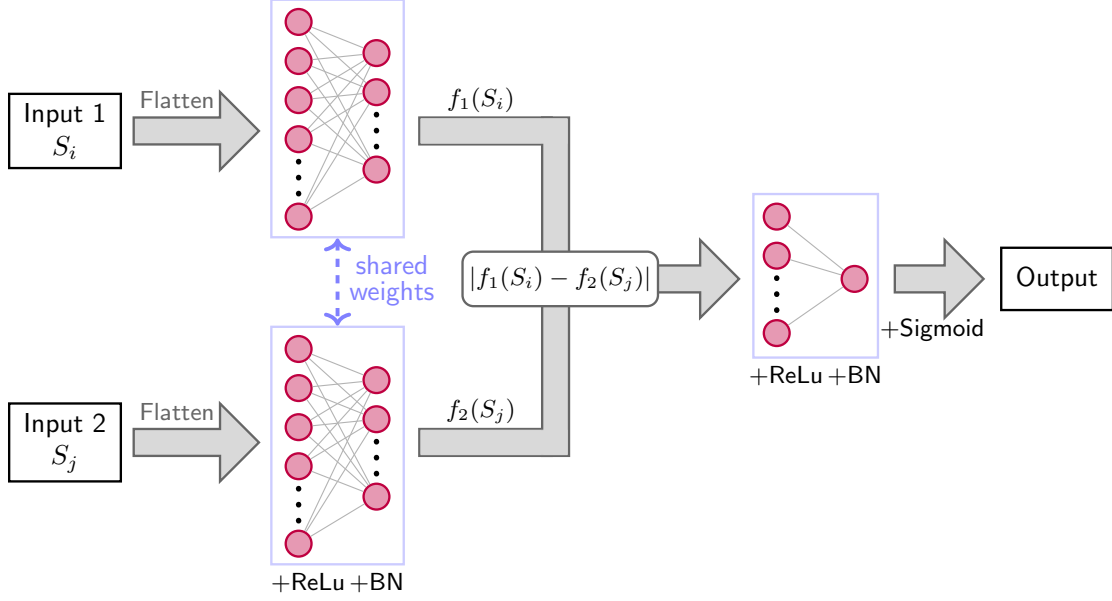


Figure 2. The structure of SNN

NN to optimize its parameters. The output of this FC layer is a feature representation f_1 of length 50. Therefore, the entire calculation process of the first branch can be expressed as function $f_1(S_i)$. Similarly, the second branch with S_j has the same process, and the feature representation is recorded as $f_2(S_j)$. Note that these two branches share the weights for learning.

The shared weights enable embedded data to be in the same space from any branches. Therefore, it allows to calculate the “distance” between two the feature representations $f_1(S_i)$ and $f_2(S_j)$, to compare the similarity of S_i and S_j . Here we define the “distance” by L_1 norm. Then this information of “distance” is fed into a dense layer of FC with the numbers of neurons 50 to 1, and this process is also attached with a *ReLU* activation function and BN. By applying a *Sigmoid* activation function to the output of FC, the result is converted into a probability of $[0, 1]$, which is regarded as classification score y , for similarity.

2.2 Data sets of the SNN

For input data of the SNN, we use the full configurations of (1+1) dimension DP (time evolution step as the characteristic temporal length.). In each lattice size $L = 8, 16, 32, 48$ and 64 , we select 101 values of $p \in [0, 1]$ uniformly and generate 1000 samples of configuration at each p . To minimize human intervention during training, we label the samples of configuration far away from the critical regime, i.e., the input configurations S_i and S_j are generated in the range of $p \in [0, 0.1] \cup [0.9, 1]$. The idea of labeling here is very different from the input of TL in Ref.²⁰. The labels “1” or “0” indicates the input data pair S_i and S_j belong to the same or different phases to ensure maximum similarity or dissimilarity between them. Specifically, if S_i and S_j both belong to $[0, 0.1]$ (or $[0.9, 1]$), the input (S_i, S_j) is labeled as “1”. Or S_i and S_j are in the range of $[0, 0.1]$ and $[0.9, 1]$ respectively, the data pair is labeled as “0”. For training, the loss function is defined as:

$$L = \sum_{i=1}^N y(S_i, S_j) \log s(S_i, S_j) + (1 - y(S_i, S_j)) \log (1 - s(S_i, S_j)), \quad (5)$$

where s is the similarity of (S_i, S_j) , and y is the label, ranging from 0 to 1. The training epoch is set to 5000, and our work is on python 3.10 and RTX 4090 Gpu partform with tensorflow 2.14.0 library.

For the process of test, a reference point, called “anchor” point, is selected to evaluate the similarity s or dissimilarity $(1 - s)$ of all configurations. The anchor p_a can be selected arbitrarily within the range of $p \in [0, 1]$. By taking the

samples of configuration at the anchor p_a as S_j and the samples of the training set as S_i , in this way the similarity between the samples at the anchor and the training samples can be estimated through the SNN. And in detail the dependence of SNN results on anchor point will be discussed in Section 3.2. Then the output of SNN, P_0 , can be expressed as two curves within bond probability $p \in [0, 1]$: the curve s of similarity and $1 - s$ of dissimilarity. The intersection of these two curves or p at $P_0 = 50\%$ represents the critical point of phase transition in the system.

3 Results

3.1 Test of the SNN framework

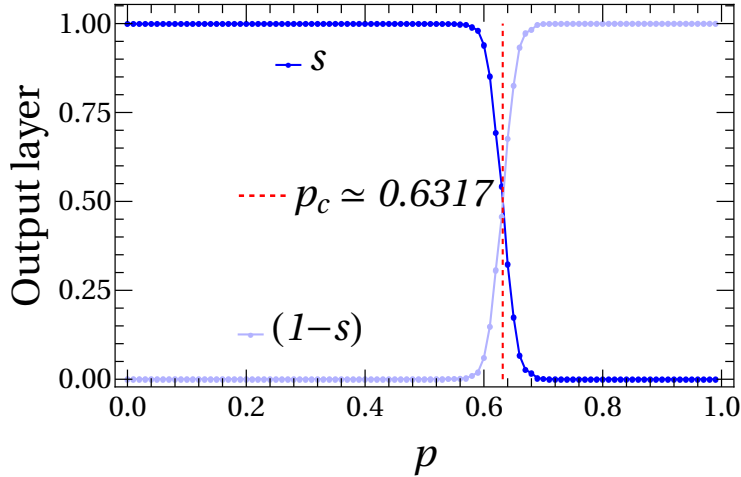


Figure 3. The output of SNN with the test anchor $p_a = 0$ at $L = 32$. The blue curve represents the similarity (s), while the ensemble average of the test samples is 1000. The light blue curve represents the non-similarity ($1 - s$).

According to the previous section, the entire SNN framework has been well trained by the set of samples within $p \in [0, 0.1] \cup [0.9, 1]$. To test the usability of SNN, firstly we select all samples of $p \in [0, 0.1]$ as S_i and only the configurations of anchor $p_a = 0$ as S_j at $L = 32$ to form the input of test. The output P_0 is shown in the figure 3. For the similar curve s , P_0 is a stable value 1 at $p \in [0, 0.48]$ and 0 at $p \in [0.64, 1]$, which means all configurations of anchor $p_a = 0$ are 100% having the same phase with samples of $p \in [0, 0.48]$ but totally different with the samples of $p \in [0.64, 1]$. In the area of $p \in (0.48, 0.64)$, the similarity curve s drops sharply, that is, the samples begin to be dissimilar to the ones of anchor $p_a = 0$, and then it is completely in differ near $p = 0.64$. The result of dissimilarity curve ($1 - s$) is opposite to the similarity. The evaluated critical point of SNN at $L = 32$ is $p_c \simeq 0.6317$, which is close to the theoretical value 0.6447³⁵. This shows that the SNN can relatively accurately predict the critical point of the (1+1) dimensional bond DP at $L = 32$ by the selected anchor $p_a = 0$.

3.2 The dependence of anchor selection

Figure. 4 shows the similarity analysis of SNN with different anchors at $L = 16, 32, 48$ and 64 . To study the dependence of anchors, we keep samples of S_i from $p \in [0, 1]$ but select anchor $p_a = 0, 0.4, 0.8$ and 1 for S_j for comparison. Since during training process the SNN learns nothing about the samples of $p_a = 0.4$ and 0.8 , here it also contains the idea of transfer learning, i.e., the range $p \in [0, 0.1] \cup [0.9, 1]$ as “source domain” and $p_a = 0.4$ or 0.8 as “target domain”. As shown in Figure. 4, the similar curve s changes with the different anchors. For $p_a = 0$ (blue curve) and 0.4 (brown curve), the similarity curve s of all configurations is from “1” to “0” at $p \in [0, 1]$, but for $p_a = 0.8$ (red curve) and 1 (green curve), it becomes the opposite trend as from “0” to “1”. Because the configurations of $p_a = 0$ and 0.4 have similar phase to the ones of $p \in [0, 0.1]$, but totally different at $p_a = 0.8$ and 1 .

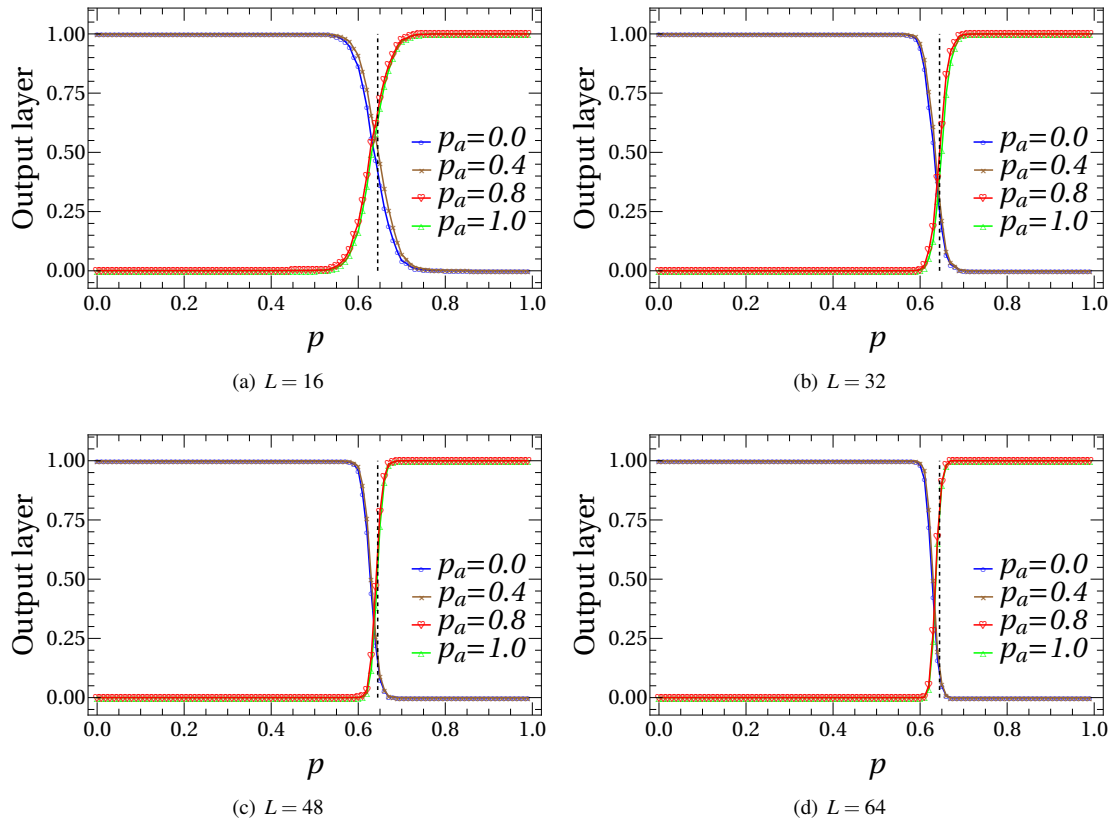


Figure 4. The output of SNN with the test anchor $p_a = 0, 0.4, 0.8$ and 1 , at different sizes (a) $L = 16$, (b) $L = 32$, (c) $L = 48$ and (d) $L = 64$.

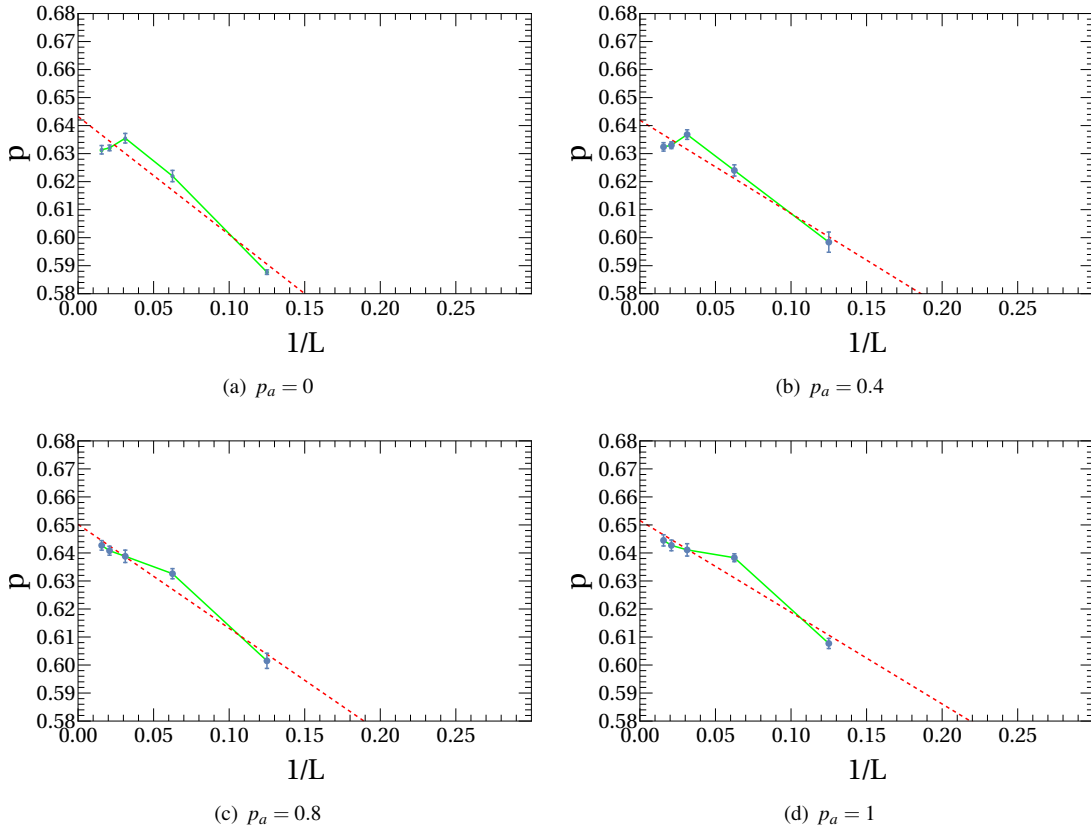


Figure 5. Extrapolation of the critical probability p_c to infinite lattice size with anchor (a) $p_a = 0$, (b) $p_a = 0.4$, (c) $p_a = 0.8$ and (d) $p_a = 1$. The predictions of this p_c^∞ are summarized in Table. 1.

3.3 Extrapolated results of critical points

To deeply analyze the dependence of the critical point predicted by SNN on anchor points, we extrapolate the results at $L = 8, 16, 32, 48$ and 64 to zero on the $1/L$ scale under anchor points $p_a = 0, 0.4, 0.8$ and 1 , by finite-size scale fitting (FSS)⁴⁸⁻⁵¹. As shown in Figure. 5, the critical values increase with the size of L , which is consistent with the layer of phase transition models under limited scale. The SNN results of p_c at infinite lattice size are summarized in Table. 1. Comparing with the theoretical value $p_c = 0.6447$ ³⁵, it shows the SNN can relatively predict critical value p_c^∞ within deviation. The closest result of SNN is $p_c = 0.6426$ at anchor $p_a = 0.4$, and the SNN results increase with the value of selected anchors, which also indicates the results of SNN may have anchor dependence. However, this anchor dependence can be diluted by expanding the training set, which will be discussed in Subsection 4.2.

Further, the curves of P_0 in Figure. 4 can be fitted with a sigmoid function:

$$p \rightarrow \frac{1}{1 + e^{-\frac{(p-p_c)}{\sigma}}} \quad \text{or} \quad p \rightarrow 1 - \frac{1}{1 + e^{-\frac{(p-p_c)}{\sigma}}}, \quad (6)$$

for $1 - s$ or s , where σ is the scaling width. As shown in Figure. 6, by the technique of data collapse we can obtain the spatial correlation exponent ν_\perp via the scaling $(p - p_c)L^{1/\nu_\perp}$. From P_0 at lattice sizes of $L = 8, 16, 32, 48$ and 64 , a proper value of ν_\perp can be found to fit the scaling. Table. 1 shows the fitted ν_\perp of each fixed anchors, all of which are consistent with the theoretical value 1.09 ³⁵. Since ν_\perp has more dependence on raw configuration and also has lower precision, it is not as sensitive to changes with the anchors as p_c^∞ .

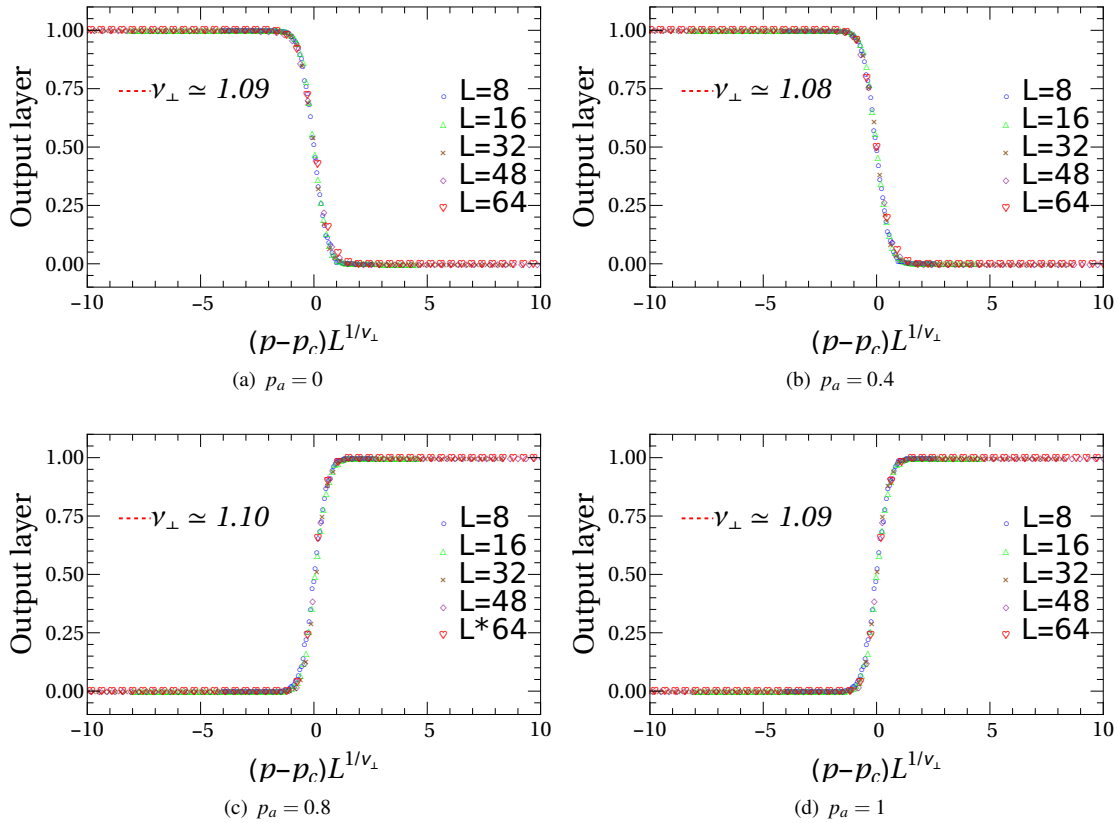


Figure 6. The collapse of the average output layer as a function of $(p - p_c)L^{1/\nu_\perp}$, with anchor (a) $p_a = 0$, (b) $p_a = 0.4$, (c) $p_a = 0.8$ and (d) $p_a = 1$.

Table 1. The critical value p_c^∞ and spatial correlation exponent ν_\perp estimated by SNN with anchor $p_a = 0, 0.4, 0.8$ and 1.

	$p_a = 0.0$	$p_a = 0.4$	$p_a = 0.8$	$p_a = 1.0$
p_c^∞	0.6411	0.6426	0.6491	0.6508
ν_\perp	1.09	1.08	1.1	1.09

4 Discussion

4.1 The anchor point $p_a = 0.64$

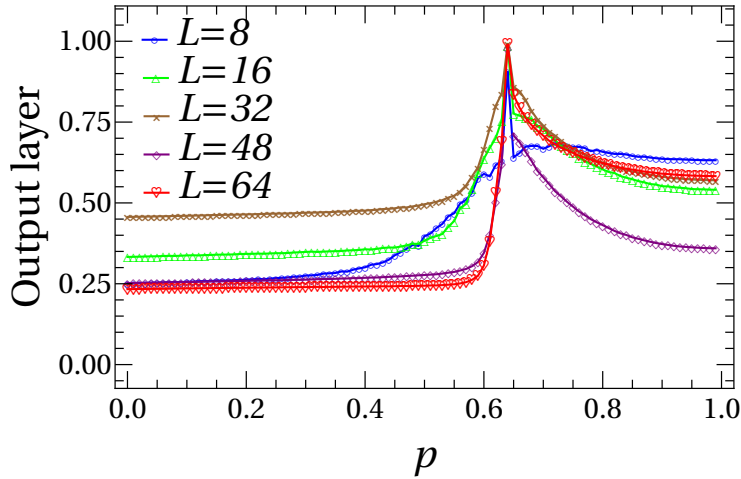


Figure 7. The output of SNN with anchor $p_a = 0.64$ at $L = 8, 16, 32, 48$ and 64.

In previous section, a series of anchor points were selected and the results proved the critical value p_c^∞ of SNN is highly dependent on anchors. To conduct more research, now we consider a special case, the anchor $p_a = 0.64$ close to the theoretical critical value 0.6447³⁵. The similarity curves of $p_a = 0.64$ at $L = 8, 16, 32, 48$ and 64 are shown in Figure 7. In this case, the curve s is a sigmoid-like function but has a structure of single peak at $p = 0.64$. The maximum values of the peak for each lattice size L are all close to 1. The reason of this behavior is that the configurations close to the critical point are only 100% similar to themselves but different from the ones of other bond probabilities. As the value of p moves away from the anchor $p_a = 0.64$, the similarity curves decrease rapidly within a short distance in the range of critical area and then changes slowly. Taking the red curve of $L = 64$ as an example, it quickly increases from $p = 0.55$ to 0.64 and suddenly drops until $p = 0.75$. These two intervals of p belong to different phases according to Figure 4, and the speed of approaching and moving away from the peak at $p = 0.64$ depends on the distance from the boundary of the critical area. This also indicates that the selection of different anchors has a significant impact on the SNN results. It also can be seen from Figure 4 that as the size L decreases, the peak drops relatively smooth, especially when $L = 8$, since for the some system sizes the information of configurations for SNN learning is insufficient.

4.2 The optimal training set

In previous tests, we sampled configurations S_i and S_j in the range of $p \in [0, 0.1] \cup [0.9, 1]$ as the training set of SNN, to minimize human intervention. However, from Section 3 it is obviously that the expected critical region is very narrow, which makes it possible to expand the training set. Typically, a wider and more accurate label training set is beneficial to improving the accuracy of NN predictions. Inspired by Ref.²⁰, an iterative approach is introduced to find an optimal interval of the training set. By defining the initial training set as $[0, l^{(0)}] \cup [r^{(0)}, 1]$ with $l^{(0)} = 0.1$ and $r^{(0)} = 0.9$, the

updating process can be started with the initial estimate critical probability $p_c^{(0)}$:

$$l^{(i+1)} = \frac{l^{(i)} + p_c^{(i)}}{2}, \quad r^{(i+1)} = \frac{r^{(i)} + p_c^{(i)}}{2}, \quad (7)$$

where i represents the i -th expansion. $p_c^{(i)}$ is the estimate critical probability by SNN on the i -th expansion. For each iteration, it has to check whether at least 99% of the output similarity in the i -th interval of training is classified as category “0” or “1”. If the condition is met, it would continue the process, otherwise make a correction like $l^{(i+1)} \rightarrow l^{(i+1)}/2$. The iteration would be stopped when the interval of training set can’t be extended any more.

In Fig. 8, we show the iteration process to achieve the estimate critical value $p_c = 0.6335$ of optimal training set $[0, 0.58] \cup [0.69, 1]$ for $L = 32$, with anchor $p_a = 0$. Obviously, the optimal training interval is much larger than the initial one, and the final result would also be more convinced. Table 2 gives the number of iterations, the optimal training interval and the critical probability predicted by SNN of $p_a = 0$ for lattice size $L = 8, 16, 32, 48$ and 64 . Then, the critical probability of infinite size can also be obtained by the extrapolation in Fig. 9(a), as $p_c^\infty = 0.6420$, and also by the data collapse we can get $v_\perp \simeq 1.09$. Table 3 shows the critical probabilities predicted by the optimal training interval under anchor point $p_a = 0, 0.4, 0.8$ and 1 . Compared to the results of initial training interval in Table 1, a larger training set makes the SNN learn features more accurate, from which the results are less affected by the selected anchor values. Based on the previous summary, it can be inferred that by using the optimal training interval, selecting any anchor in training interval as test sample set can predict a reliable result. On the other hand, Table 3 also lists the results of supervised learning⁴⁷, autoencoder (AE)⁴⁷ and DANN²⁰ for comparison.

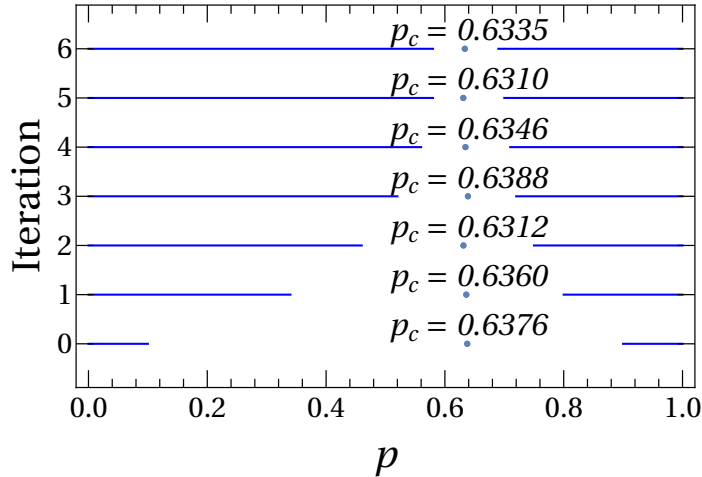


Figure 8. Evolution of the training set, and the corresponding critical bond probability values.

Table 2. The optimal training interval of $L = 8, 16, 32, 48$ and 64 , with iteration step and predicted p_c at each size.

Lattice size	Iteration step	Optimal training interval	p_c
$L = 8$	2	$[0, 0.18] \cup [0.82, 1]$	0.6006
$L = 16$	6	$[0, 0.53] \cup [0.73, 1]$	0.6258
$L = 32$	6	$[0, 0.58] \cup [0.69, 1]$	0.6335
$L = 48$	6	$[0, 0.59] \cup [0.67, 1]$	0.6323
$L = 64$	6	$[0, 0.60] \cup [0.67, 1]$	0.6357

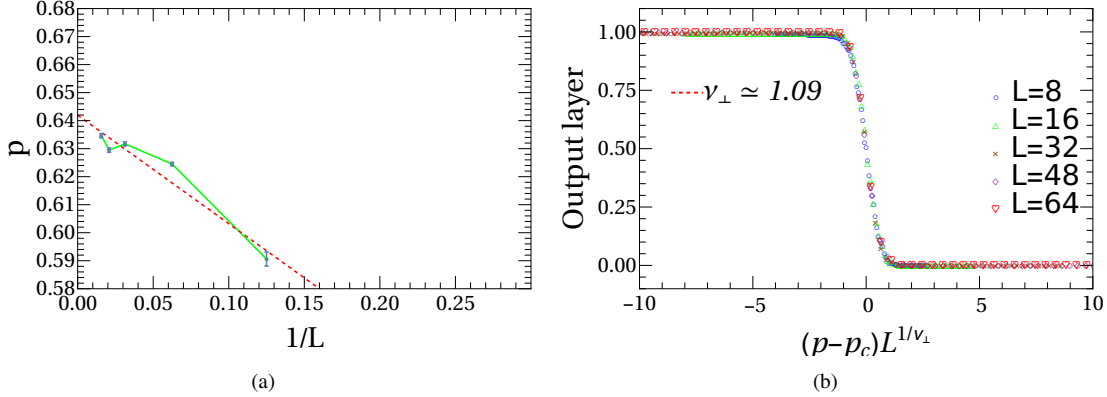


Figure 9. (a) Extrapolation of the critical probability p_c to infinite lattice size with $p_a = 0$, by the optimal training intervals in Table 3. (b) The collapse of the average output layer as a function of $(p - p_c)L^{1/v_\perp}$.

Table 3. Comparing the supervised machine learning, autoencoder (AE), domain adversarial neural network (DANN), and SNN methods for calculating the critical value p_c^∞ and spatial correlation exponent v_\perp with optimal training intervals.

Method	Supervised ⁴⁷	AE ⁴⁷	DANN ²⁰	$p_a = 0.0$	$p_a = 0.4$	$p_a = 0.8$	$p_a = 1.0$
p_c^∞	0.6408	0.643(2)	0.6453(5)	0.6420	0.6429	0.6452	0.6440
v_\perp	1.09(2)	None	1.09(6)	1.09	1.08	1.1	1.09

5 Conclusion

In this paper, we have applied the Siamese Neural Network (SNN) on the (1+1)-dimensional bond directed percolation to study its critical behaviors of nonequilibrium system. Here the SNN is used as a semi-supervised learning method, in which the key information of critical behavior can be predicted by labeling only a part of raw configurations as input for training. And the output of the SNN is similarity, which transforms the classification problems of phase transition into a discussion of difference, broadening the application of Machine learning (ML) techniques in the study of critical behaviors.

By the output similarity of SNN, we predict the critical points of the system at different lattice sizes, and then use the fitting based on finite-size scaling to obtain the theoretical values at unlimited system. Further, the curve of similarity also can be fit to a sigmoid-like function, which allows us to calculate the spatial correlation exponent v_\perp of non-equilibrium phase transition system through data collapse.

During the test, the selection of anchor points is of particular importance. By selecting the same training set, we discussed the impact of configurations under different anchors on the results. As the chosen anchor is outside the critical area, the predicted critical point increases with the value of anchor. For the anchor close to critical point, the curve of similarity shows a structure of single peak at the anchor, which indicates these configurations at the anchor only 100% similar to themselves. In this case, the critical point cannot be predicted by the SNN. To make the calculation more efficient and reduce anchor dependence, we optimize the training interval through an iterative method. After optimization, the critical point result obtained by SNN is very accurate, comparable to the results of traditional supervised learning, AE and DANN.

With the widespread utilization of machine learning techniques in the fields of statistics and condensed matter physics, it is a promising future for further advancements. The SNN approach introduced in this research paper has the potential to offer novel insights into the exploration of DP and Ising-like phase transitions.

Acknowledgements

This work was supported in part by National Research Incubation Fund of Baoshan University(BYPY202216), the Baoshan University Doctoral Research Initiation Fund Project(BSKY202305), Academician workstation of Wengbangchun, Yunnan Province(Grant No.202205AF150032), Youth project of Yunnan Province Science and Technology Department(202401AU070035), Key Laboratory of Quark and Lepton Physics (MOE), Central China Normal University(Grant No.QLPL2022P01), and China Scholarship Council (CSC) - Swansea University scholarship.

References

1. Jordan, M. I. & Mitchell, T. M. Machine learning: Trends, perspectives, and prospects. *Science* **349**, 255–260, DOI: [10.1126/science.aaa8415](https://doi.org/10.1126/science.aaa8415) (2015).
2. Mohri, M., Rostamizadeh, A. & Talwalkar, A. *Foundations of machine learning* (MIT press, 2018).
3. Mehta, P. & Schwab, D. J. An exact mapping between the variational renormalization group and deep learning. *arXiv preprint arXiv:1410.3831* (2014).
4. Carleo, G. & Troyer, M. Solving the quantum many-body problem with artificial neural networks. *Science* **355**, 602–606 (2017).
5. Carrasquilla, J. & Melko, R. G. Machine learning phases of matter. *Nat. Phys.* **13**, 431–434 (2017).
6. Wang, L. Discovering phase transitions with unsupervised learning. *Phys. Rev. B* **94**, 195105 (2016).
7. Van Nieuwenburg, E. P., Liu, Y.-H. & Huber, S. D. Learning phase transitions by confusion. *Nat. Phys.* **13**, 435–439 (2017).
8. van Nieuwenburg, E., Bairey, E. & Refael, G. Learning phase transitions from dynamics. *Phys. Rev. B* **98**, 060301 (2018).
9. Canabarro, A., Fanchini, F. F., Malvezzi, A. L., Pereira, R. & Chaves, R. Unveiling phase transitions with machine learning. *Phys. Rev. B* **100**, 045129 (2019).
10. Ni, Q., Tang, M., Liu, Y. & Lai, Y.-C. Machine learning dynamical phase transitions in complex networks. *Phys. Rev. E* **100**, 052312 (2019).
11. Wang, Y., Li, W., Liu, F. & Shen, J. Supervised and unsupervised learning of (1+1)-dimensional even-offspring branching annihilating random walks (2023). [2307.05618](https://arxiv.org/abs/2307.05618).
12. Wetzel, S. J. Unsupervised learning of phase transitions: From principal component analysis to variational autoencoders. *Phys. Rev. E* **96**, 022140, DOI: [10.1103/PhysRevE.96.022140](https://doi.org/10.1103/PhysRevE.96.022140) (2017).
13. Hu, W., Singh, R. R. & Scalettar, R. T. Discovering phases, phase transitions, and crossovers through unsupervised machine learning: A critical examination. *Phys. Rev. E* **95**, 062122 (2017).
14. Wang, J., Zhang, W., Hua, T. & Wei, T.-C. Unsupervised learning of topological phase transitions using the calinski-harabaz index. *Phys. Rev. Res.* **3**, 013074 (2021).
15. Käming, N. *et al.* Unsupervised machine learning of topological phase transitions from experimental data. *Mach. Learn. Sci. Technol.* **2**, 035037 (2021).
16. Shen, J. *et al.* Machine learning of pair-contact process with diffusion. *Sci. Reports* **12**, 19728, DOI: [10.1038/s41598-022-23350-2](https://doi.org/10.1038/s41598-022-23350-2) (2022).
17. El Alaoui, A., Cheng, X., Ramdas, A., Wainwright, M. J. & Jordan, M. I. Asymptotic behavior of ℓ_p -based laplacian regularization in semi-supervised learning. In *Conference on Learning Theory*, 879–906 (PMLR, 2016).
18. Bencteux, V. *et al.* Automatic task recognition in a flexible endoscopy benchtop trainer with semi-supervised learning. *Int. J. Comput. Assist. Radiol. Surg.* **15**, 1585–1595 (2020).
19. Court, C. J. & Cole, J. M. Auto-generated materials database of curie and néel temperatures via semi-supervised relationship extraction. *Sci. data* **5**, 1–12 (2018).
20. Shen, J. *et al.* Transfer learning of phase transitions in percolation and directed percolation. *Phys. Rev. E* **105**, 064139, DOI: [10.1103/PhysRevE.105.064139](https://doi.org/10.1103/PhysRevE.105.064139) (2022).

21. Chen, X. *et al.* Study of phase transition of potts model with domain adversarial neural network. *Phys. A: Stat. Mech. its Appl.* **617**, 128666, DOI: <https://doi.org/10.1016/j.physa.2023.128666> (2023).
22. Wang, L. Discovering phase transitions with unsupervised learning. *Phys. Rev. B* **94**, 195105, DOI: [10.1103/PhysRevB.94.195105](https://doi.org/10.1103/PhysRevB.94.195105) (2016).
23. Ch'ng, K., Vazquez, N. & Khatami, E. Unsupervised machine learning account of magnetic transitions in the hubbard model. *Phys. Rev. E* **97**, 013306, DOI: [10.1103/PhysRevE.97.013306](https://doi.org/10.1103/PhysRevE.97.013306) (2018).
24. Chicco, D. Siamese neural networks: An overview. *Artif. neural networks* 73–94 (2021).
25. Ranasinghe, T., Orašan, C. & Mitkov, R. Semantic textual similarity with siamese neural networks. In *Proceedings of the International Conference on Recent Advances in Natural Language Processing (RANLP 2019)*, 1004–1011 (2019).
26. Zhang, C., Liu, W., Ma, H. & Fu, H. Siamese neural network based gait recognition for human identification. In *2016 IEEE International Conference on Acoustics, Speech and Signal Processing (ICASSP)*, 2832–2836 (IEEE, 2016).
27. Wu, H., Xu, Z., Zhang, J., Yan, W. & Ma, X. Face recognition based on convolution siamese networks. In *2017 10th International Congress on Image and Signal Processing, BioMedical Engineering and Informatics (CISP-BMEI)*, 1–5 (IEEE, 2017).
28. Bertinetto, L., Valmadre, J., Henriques, J. F., Vedaldi, A. & Torr, P. H. Fully-convolutional siamese networks for object tracking. In *Computer Vision—ECCV 2016 Workshops: Amsterdam, The Netherlands, October 8–10 and 15–16, 2016, Proceedings, Part II 14*, 850–865 (Springer, 2016).
29. Qi, Y., Song, Y.-Z., Zhang, H. & Liu, J. Sketch-based image retrieval via siamese convolutional neural network. In *2016 IEEE International Conference on Image Processing (ICIP)*, 2460–2464 (IEEE, 2016).
30. Ichida, A. Y., Meneguzzi, F. & Ruiz, D. D. Measuring semantic similarity between sentences using a siamese neural network. In *2018 International Joint Conference on Neural Networks (IJCNN)*, 1–7 (IEEE, 2018).
31. Patel, Z., Merali, E. & Wetzels, S. J. Unsupervised learning of rydberg atom array phase diagram with siamese neural networks. *New J. Phys.* **24**, 113021 (2022).
32. Obukhov, S. The problem of directed percolation. *Phys. A: Stat. Mech. its Appl.* **101**, 145–155 (1980).
33. Grimmett, G. & Hiemer, P. Directed percolation and random walk. In *In and Out of Equilibrium: Probability with a Physics Flavor*, 273–297 (Springer, 2002).
34. Henkel, M. *Non-equilibrium phase transitions* (Springer, 2008).
35. Hinrichsen, H. Non-equilibrium critical phenomena and phase transitions into absorbing states. *Adv. Phys.* **49**, 815–958, DOI: [10.1080/00018730050198152](https://doi.org/10.1080/00018730050198152) (2000).
36. Ódor, G. Universality classes in nonequilibrium lattice systems. *Rev. Mod. Phys.* **76**, 663–724, DOI: [10.1103/RevModPhys.76.663](https://doi.org/10.1103/RevModPhys.76.663) (2004).
37. LÜBECK, S. Universal scaling behavior of non-equilibrium phase transitions. *Int. J. Mod. Phys. B* **18**, 3977–4118, DOI: [10.1142/S0217979204027748](https://doi.org/10.1142/S0217979204027748) (2004).
38. Bhattacharjee, S. M. & Seno, F. A measure of data collapse for scaling. *J. Phys. A: Math. Gen.* **34**, 6375 (2001).
39. Kimchi, I., Shekelton, J. P., McQueen, T. M. & Lee, P. A. Scaling and data collapse from local moments in frustrated disordered quantum spin systems. *Nat. communications* **9**, 4367 (2018).
40. Grassberger, P. On the critical behavior of the general epidemic process and dynamical percolation. *Math. Biosci.* **63**, 157–172 (1983).
41. Von Niessen, W. & Blumen, A. Dynamics of forest fires as a directed percolation model. *J. Phys. A: Math. Gen.* **19**, L289 (1986).
42. Nagatani, T. Jamming transition in the traffic-flow model with two-level crossings. *Phys. Rev. E* **48**, 3290 (1993).
43. De'Bell, K. & Essam, J. Directed percolation: mean field theory and series expansions for some two-dimensional lattices. *J. Phys. A: Math. Gen.* **16**, 385 (1983).

44. Kinzel, W. & Yeomans, J. Directed percolation: a finite-size renormalisation group approach. *J. Phys. A: Math. Gen.* **14**, L163 (1981).
45. Janssen, H.-K. & Täuber, U. C. The field theory approach to percolation processes. *Annals Phys.* **315**, 147–192 (2005).
46. Hinrichsen, H. & Koduvely, H. M. Numerical study of local and global persistence in directed percolation. *The Eur. Phys. J. B-Condensed Matter Complex Syst.* **5**, 257–264 (1998).
47. Shen, J., Li, W., Deng, S. & Zhang, T. Supervised and unsupervised learning of directed percolation. *Phys. Rev. E* **103**, 052140, DOI: [10.1103/PhysRevE.103.052140](https://doi.org/10.1103/PhysRevE.103.052140) (2021).
48. Binder, K. Finite size effects on phase transitions. *Ferroelectrics* **73**, 43–67 (1987).
49. Fisher, M. E. & Barber, M. N. Scaling theory for finite-size effects in the critical region. *Phys. Rev. Lett.* **28**, 1516 (1972).
50. Privman, V. & Fisher, M. E. Finite-size effects at first-order transitions. In *Current Physics—Sources and Comments*, vol. 2, 149–181 (Elsevier, 1988).
51. Fan, S. & Zhong, F. Determination of the dynamic and static critical exponents of the two-dimensional three-state potts model using linearly varying temperature. *Phys. Rev. E* **76**, 041141 (2007).